

Non-Thermal Radio and Gamma-Ray Emission from a Supernova Remnant by the Blast Wave Breaking Out of the Circumstellar Matter

Takafumi SHIMIZU¹, Kuniaki MASAI¹, and Katsuji KOYAMA^{2,3}

¹Department of Physics, Tokyo Metropolitan University, 1-1 Minami-Ohsawa, Hachioji, Tokyo 192-0397
t-shimizu@phys.se.tmu.ac.jp

²Department of Physics, Graduate school of Science, Kyoto University, Oiwake-cho, Kitashirakawa, Kyoto 606-8502

³Department of Earth and Space Science, Graduate School of Science, Osaka University, 1-1 Machikaneyama, Toyonaka, Osaka 560-0043

(Received ; accepted)

Abstract

We calculate synchrotron radio emission and γ -ray emission due to bremsstrahlung, inverse-Compton scattering and π^0 -decay from the remnant of supernova which exploded in the circumstellar matter (CSM) formed by the progenitor's stellar wind. This sort of situation is a possible origin of mixed-morphology supernova remnants (SNRs) like W49B, which exhibit recombination-radiation spectra in X-ray emission. We assume that the CSM of $1.5 M_{\odot}$ exists at 0.07–3 pc away from the supernova in the interstellar medium (ISM) of density 0.016 cm^{-3} . When the blast wave breaks out of the CSM into the ISM, its velocity rapidly increases and hence particle acceleration is enhanced. The maximum energy of protons reaches $\sim 1300 \text{ TeV}$ just after the break-out with $\sim 0.5\%$ of the explosion energy. We consider the non-thermal emission from the blast-shocked ISM shell after the break-out. Synchrotron radio flux at 1 GHz is tens Jy, comparable to the observed from mixed-morphology SNRs. Because of low density, the γ -ray luminosity is dominated by inverse-Compton scattering, which is higher than the π^0 -decay luminosity by an order of magnitude. The total γ -ray luminosity including bremsstrahlung is of the order of $10^{33} \text{ erg s}^{-1}$ lower than the typical value $10^{35}\text{--}10^{36} \text{ erg s}^{-1}$ observed from mixed-morphology SNRs. However, if, e.g., $\sim 10\%$ of accelerated protons interact with some matter of density $\sim 100 \text{ cm}^{-3}$, π^0 -decay γ -ray luminosity would be enhanced to be comparable with the observed value.

Key words: stars: circumstellar matter - ISM: supernova remnants

1. Introduction

About 70% of Galactic supernova remnants (SNRs) exhibit shell-like morphology in radio wavelength (Green 2009). The radio shells are due to synchrotron emission by non-thermal electrons of order of GeV. Many of these SNRs also exhibit shell-like morphology in X-rays, due to bremsstrahlung and line emission by thermal electrons of order of keV. The electrons are heated and/or accelerated by interstellar shocks of SNRs. On the other hand, $\sim 10\%$ of the SNRs that have the radio shells exhibit center-filled thermal X-rays, and are called mixed-morphology (MM) SNRs (e.g., Rho & Petre 1998). Recently, *Suzaku* revealed recombination radiation, which are hardly expected for typical shell-like SNRs, in X-ray spectra of six MM SNRs so far observed: IC443 (Yamaguchi et al. 2009), W49B (Ozawa et al. 2009), G359.1-0.5 (Ohnishi et al. 2011), W28 (Sawada & Koyama 2012), W44 (Uchida et al. 2012), and G346.6-0.2 (Yamauchi et al. 2012).

MM SNRs are characteristic also in γ -ray emission. *Fermi* detected GeV γ -rays from SNRs: while the luminosities in the 1–100 GeV band of shell-like SNRs are $10^{33}\text{--}10^{35} \text{ erg s}^{-1}$ (Abdo et al. 2010b, Castro & Slane 2010, Katagiri et al. 2011, Abdo et al. 2011, Giordano et al. 2011, Tanaka et al. 2011), the luminosities of MM SNRs are distinctively higher, $10^{35}\text{--}10^{36} \text{ erg s}^{-1}$ (Abdo et

al. 2009, Abdo et al. 2010a, Abdo et al. 2010c, Abdo et al. 2010d, Abdo et al. 2010e, Castro & Slane 2010). This may imply that such intense γ -rays come from the dense matter around MM SNRs. Actually, for these MM SNRs, interaction with molecular clouds is suggested by 1720 MHz OH maser (Frail et al. 1994, Yusef-Zadeh et al. 1995, Frail et al. 1996, Green et al. 1997, Claussen et al. 1997, Hewitt & Yusef-Zadeh 2009) and/or near-infrared observations (Keohane et al. 2007). The γ -ray spectra of observed SNRs are not always single power-laws but exhibit a break at an energy of $\sim 1\text{--}5 \text{ GeV}$ above which their slopes are steepen.

X-ray characteristics different than shell-like SNRs and possible interaction with molecular clouds may suggest that MM SNRs are remnants of core-collapse explosion of massive stars surrounded by HII regions, stellar wind matter, and molecular clouds, as in star-forming regions. Recombination radiation in X-rays are predicted by Itoh & Masai (1989) for the remnant of a supernova surrounded by its progenitor's stellar wind matter. They show the X-ray spectra due to rarefaction (adiabatic cooling) caused when the blast wave breaks out of the wind matter to expand rapidly into the ambient interstellar medium. Recently, Shimizu, Masai & Koyama (2012), hereafter Paper I, extend this work to non-spherically-symmetric stellar wind matter, and find that recomb-

nation X-rays exhibit center-filled morphology like MM SNRs with various shapes depending on the viewing direction. They also suggest that synchrotron radio shell is located outside, surrounding the X-ray emitting region.

If rarefaction caused by the shock break-out is the origin of recombination X-rays found in MM SNRs, it is naturally of our interest whether the SNR model can explain observed radio and γ -ray emissions as well. Hence, in the present paper, we investigate non-thermal particles, which can be accelerated by the shock of the SNR model in Paper I, and emission thereby from the blast-shocked ISM shell. In the following section, we describe the SNR model in Paper I and the particle acceleration. In Section 3 we show calculations of non-thermal radio flux and γ -ray luminosity, and discuss the results in Section 4.

2. Model

2.1. Supernova remnant

We consider model B2 of Paper I for a model of MM SNR. The model describes evolution that the initially spherically-symmetric ejecta interact with anisotropic circumstellar matter (CSM). Outside the CSM, a uniform interstellar medium (ISM) of density 0.016 cm^{-3} is assumed. Such low density can be possible for an H II region formed by the progenitor. The ejecta have an initial kinetic energy of $2 \times 10^{51} \text{ erg}$ and a mass of $10 M_{\odot}$, and therefore the initial velocity of the blast wave is $8.5 \times 10^3 \text{ km s}^{-1}$. For comparison, we also calculate the evolution of SNR without CSM, which expands directly into the uniform ISM of the same density.

The CSM is composed of the stellar wind matter blown by the progenitor in its pre-supernova phase. If the progenitor rotated rapidly, the stellar wind may have an anisotropic density distribution. We assume that the CSM is concentrated in the equatorial plane. The density on the equatorial plane is 4 times higher than that in the polar direction at the same radius. The mass-loss rate is $5 \times 10^{-5} M_{\odot} \text{ yr}^{-1}$ at a wind velocity of 100 km s^{-1} . The inner and outer radii of the CSM are 0.07 pc and 3 pc in the equatorial direction. These radii imply that the wind activity lasts 3×10^4 years and then ceases 6×10^2 years before the explosion. The mass of the CSM is $1.5 M_{\odot}$, which is obtained from the period of the wind activity and the mass-loss rate.

The wind parameters can be possible for B[e] supergiants or luminous blue variables (LBVs). For example, radio observations suggest that W9, which is a B[e] supergiant in Westerlund 1, has the wind velocity of $\sim 10^2 \text{ km s}^{-1}$ and the mass-loss rate of $\sim 10^{-4} M_{\odot} \text{ yr}^{-1}$ (Dougherty et al. 2010). LBVs have typically the wind velocity of $\sim 10^2 \text{ km s}^{-1}$ and the mass-loss rate of $\sim 10^{-5} - 10^{-4} M_{\odot} \text{ yr}^{-1}$ (Humphreys & Davidson 1994). Although LBVs were considered not to explode as supernova, recent observation shows that a progenitor of SN 2005gl is a LBV (Gal-Yam et al. 2007). Also, observations of type IIn supernovae suggest the interaction between ejecta and dense CSM, which have the wind velocity of $\sim 10^2 - 10^3 \text{ km s}^{-1}$ and the mass-loss rate of

$\sim 10^{-4} - 1 M_{\odot} \text{ yr}^{-1}$ (e.g., Kiewe et al. 2012).

The blast wave breaks out of the CSM at $\sim 450 \text{ yr}$ in the equatorial direction, and then is rapidly accelerated. Rarefaction wave propagates inward from CSM-ISM contact interface. This causes rapid adiabatic expansion and thus cooling of the once-shocked CSM and ejecta, and results in recombination-radiation X-rays. Since the ISM is rarefied enough to make a density difference of factor ~ 10 at the CSM-ISM interface, rarefaction occurs for the mass loss rate $5 \times 10^{-5} M_{\odot} \text{ yr}^{-1}$ assumed here (cf. Moriya 2012). After that, blast wave propagates to form a shocked shell into the ISM, while the second reverse-shock propagates inward. Figure 1 shows a snap shot, density map of the shocked matter averaged over the line of sight, of the model SNR. The inner black lines represent the reverse-shocked ejecta which is bright in thermal X-rays, and the outer gray lines represent the blast-shocked ISM which is faint in X-rays but can be bright in radio. The late time evolution of the blast wave approaches that of the model without CSM, as shown by Itoh & Masai (1989).

Figure 2 shows the blast-wave radius R_b , velocity V_s , mean temperatures $\langle T_p \rangle$ of protons and $\langle T_e \rangle$ of electrons, and mean number density $\langle n \rangle$ of the blast-shocked ISM. The proton and electron temperatures are calculated from the temperatures $kT_{p,e} \propto m_{p,e} V_s^2$ at the shock front, assuming the energy transport from protons to electrons through Coulomb collisions in the post-shock region (Masai 1994; see also Paper I), where m_p and m_e are the mass of proton and electron, respectively.

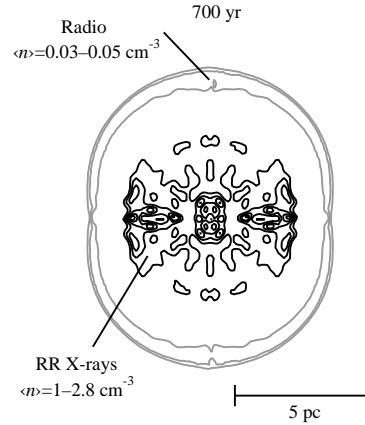


Fig. 1. Contours of the number density of shocked matter averaged over line of sight in the equatorial plane of model B2 at 700 yr. Black lines represent those for reverse-shocked ejecta. Gray lines represent those for the shocked ISM. “RR X-rays” means recombination-radiation X-rays.

2.2. Particle acceleration

We consider diffusive shock acceleration by the blast wave: part of thermal particles of the shocked ISM are scattered across the shock by magnetic inhomogeneities and gain momentum. The energy spectrum of accelerated

particles is expressed in a form (Bell 1978)

$$N(E) = K(E + mc^2)(E^2 + 2mc^2E)^{-(\mu+1)/2} \quad (1)$$

with

$$K = \xi \langle n \rangle (\mu - 1) (E_{\text{inj}}^2 + 2mc^2 E_{\text{inj}})^{(\mu-1)/2} \quad (2)$$

for $E_{\text{inj}} \leq E \leq E_{\text{max}}$. Here, $E = (\gamma - 1)mc^2$ is the kinetic energy of the particle of mass m with the Lorentz factor γ , E_{inj} is the injection kinetic energy, E_{max} is the maximum kinetic energy of accelerated particles, and ξ is the injection efficiency. The injection efficiency is defined as the ration of the number density of accelerated to thermal particles.

The diffusive shock acceleration results in a single power-law energy spectrum, as described above. On the other hand, γ -ray observations of SNRs suggest that the energy spectrum of particles is not simply a single power-law, but, for instance, *Fermi*-observed SNRs show a break at an energy of $\sim 1\text{--}5$ GeV, as mentioned in Section 1. Since cooling time at the break energy is much longer than the age, this break may reflect acceleration processes. Therefore, for the energy spectrum of accelerated particles we assume a broken power-law

$$N(E) = \begin{cases} KE^{-\mu}, & \text{for } E < E_b, \\ KE_b^{-\mu+\mu_2} E^{-\mu_2}, & \text{for } E \geq E_b, \end{cases} \quad (3)$$

where E_b is the break energy of 10 GeV, taken so as to make a GeV break in the γ -ray spectrum. The spectral indexes are assumed to be $\mu = 2$ and $\mu_2 = 2.3$, which is a medium value of spectral index of cosmic-ray sources (e.g., Putze et al. 2011).

For the injection energy E_{inj} and efficiency ξ , we consider that particles in the high energy tail of the thermal distribution are injected into acceleration process, as

$$E_{\text{inj-p,e}} = \lambda_{\text{p,e}} k T_{\text{p,e}}. \quad (4)$$

with a constant λ , where the characters “p” and “e” mean proton and electron, respectively. Then a relation between ξ and λ is given by

$$\begin{aligned} \xi_{\text{p,e}} &\equiv \frac{\int_{E_{\text{inj-p,e}}}^{\infty} f_{\text{p,e}}(E) dE}{\int_0^{\infty} f_{\text{p,e}}(E) dE} \\ &= 1 - \text{erf}(\lambda_{\text{p,e}}^{1/2}) + \frac{2}{\pi^{1/2}} \lambda_{\text{p,e}}^{1/2} e^{-\lambda_{\text{p,e}}}, \end{aligned} \quad (5)$$

where $f(E)$ is the Maxwellian distribution function, and erf is the error function.

We determine ξ_p for the pressure of accelerated protons to be equal to 10% of the ram pressure of ISM enters in the blast wave. The pressure of accelerated particles is given by

$$\begin{aligned} P_{\text{CR}} &= \frac{1}{3} \int_{p_{\text{inj}}}^{p_{\text{max}}} N'(p) p v dp \\ &\simeq \frac{1}{3} \xi \langle n \rangle c p_{\text{inj}} \left[\ln \left(\frac{2p_b}{mc} \right) + \frac{1}{\mu_2 - 2} \left(\frac{p_b c}{E_b} \right)^{-\mu_2 + 2} \right], \end{aligned} \quad (6)$$

where we use $\mu = 2$ in the last expression. Here, v is the particle velocity, p is the momentum of a particle,

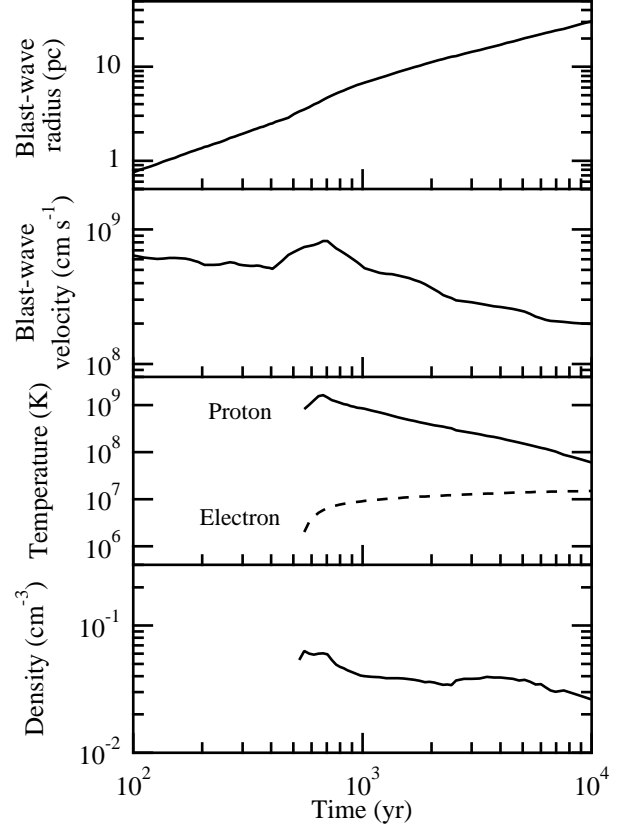


Fig. 2. From top to bottom, evolutions of the blast-wave radius, the blast-wave velocity, the proton and electron temperatures averaged over the blast-shocked ISM in the equatorial direction, and the number density averaged over the blast-shocked ISM in the equatorial direction, as functions of the elapsed time after explosion.

$p_{\text{inj}} = (2mE_{\text{inj}})^{1/2}$ is the injection momentum, $p_{\text{max}} = E_{\text{max}}/c$ is the maximum momentum, p_b is the break momentum, and $N'(p)dp = N(E)dE$. In the last expression in equation (6), $p_{\text{inj}} \ll mc$ and $p_{\text{max}} \gg p_b > mc$ are considered. The injection efficiency of protons is roughly proportional to the blast-wave velocity V_s because $\xi_p \propto V_s^2/p_{\text{inj-p}} \propto V_s^2/T_p^{1/2} \propto V_s$. The injection efficiency of protons reaches the maximum $\sim 2 \times 10^{-4}$ at ~ 530 yr, and then decreases to 5×10^{-5} at ~ 10000 yr. We determine ξ_e for the pressure $P_{\text{CR-e}}$ of accelerated electrons not to exceed the pressure $P_{\text{CR-p}}$ of accelerated protons. The ratio of the pressure of accelerated electrons to protons is

$$\frac{P_{\text{CR-e}}}{P_{\text{CR-p}}} \simeq 0.05 \frac{\xi_e}{\xi_p} \left(\frac{E_{\text{inj-e}}}{E_{\text{inj-p}}} \right)^{1/2}. \quad (7)$$

If the injection energy of electrons is the same as protons, $\xi_e \lesssim 20 \xi_p$ follows. In the following, we express ξ_e in unit of ξ_p .

The maximum energy E_{max} is determined by the time-scales of energy gain and loss. Adiabatic loss due to SNR expansion is negligible through the age concerned here. The dominant loss process is synchrotron radiation and inverse-Compton scattering for electrons. Assuming that

1) mean free path of a particle is its gyration radius (Bohm limit), 2) shock compression ratio is 4, and 3) accelerated particles are relativistic ($\gamma \gg 1$), we estimate the time-scales of acceleration and radiation loss as

$$t_{\text{acc}} \simeq \frac{32\gamma mc^3}{3eBV_s^2} \quad (8)$$

and

$$t_{\text{loss(electron)}} \simeq \frac{6\pi me c}{\gamma \sigma_T (B^2 + 8\pi U_{\text{CMB}})}, \quad (9)$$

respectively, where σ_T is the Thomson scattering cross section, e is the elementary electric charge, B is the strength of the magnetic field in the shock downstream, assumed to be 4 times the strength in the upstream, and U_{CMB} is the energy density of cosmic microwave background. In SNRs, the magnetic field strength can be stronger than the average interstellar value by magnetic amplification mechanisms, as suggested by X-ray variability of RX J1713.7-3946 (Uchiyama et al. 2007). Using the equation (14) of Bell & Lucek (2001), we calculate the field strength in the SNR evolution. The magnetic amplification may cause the non-linear feedback from accelerated particles to the shock structure. However, such feedback is small when the injection efficiency is lower than $\sim 10^{-4}$ (e.g., Ferrand et al. 2010), which is marginally attained after the blast-wave break-out concerned here.

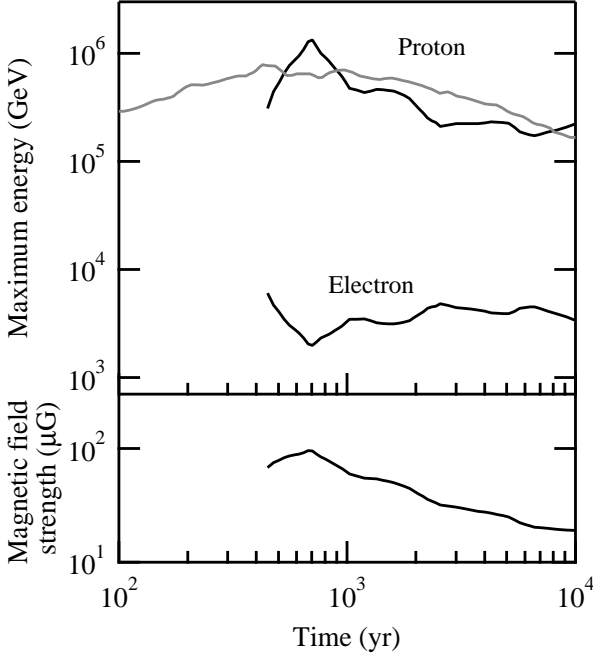


Fig. 3. Maximum energy that the accelerated protons and electrons can reach at a given time (*upper*) and the magnetic field strength in the shock downstream (*lower*), as functions of the elapsed time after explosion. Gray line represents the maximum energy of the protons in the SNR evolution without CSM.

In Figure 3 we show the time evolution of E_{max} and B . For protons E_{max} is determined by $t_{\text{acc}} \sim t_{\text{age}}$ and reaches

~ 1300 TeV at ~ 700 yr, while ~ 800 TeV at ~ 430 yr in the case without CSM. For electrons E_{max} is determined by $t_{\text{acc}} \sim t_{\text{loss(electron)}}$, and its maximum is about 10 TeV at the moment of the break-out. At ~ 700 yr just after the break-out, E_{max} takes its maximum/minimum for protons/electrons because of rapid increase of the shock velocity and magnetic field. For the explosion energy 2×10^{51} erg assumed, the total energy of accelerated protons is 1×10^{49} erg at ~ 700 yr and $\sim 2 \times 10^{50}$ erg at ~ 10000 yr.

3. Non-thermal radiation

We calculate the non-thermal emission from the blast-shocked ISM shell, in which accelerated particles are confined for the either shorter time, t_{age} or R_b^2/D . Here D is the diffusion coefficient and taken to be in the form $D_{10}(E/10 \text{ GeV})(B/10 \mu\text{G})^{-1} \text{ cm}^2 \text{ s}^{-1}$ with a numerical coefficient D_{10} . Observations of cosmic-rays suggest that $D \sim 10^{28} \text{ cm}^2 \text{ s}^{-1}$ at 10 GeV (Berezinskii et al. 1990). On the other hand, near SNRs, GeV and TeV observations suggest $D \sim 10^{26} \text{ cm}^2 \text{ s}^{-1}$ at 10 GeV (e.g., Li & Chen 2012). We adopt $D_{10} = 3 \times 10^{27}$ so that $D \sim 10^{28} \text{ cm}^2 \text{ s}^{-1}$ for $B = 3 \mu\text{G}$, typical field in the interstellar space, and $D \sim 10^{26} \text{ cm}^2 \text{ s}^{-1}$ for $B \sim 100 \mu\text{G}$, which could be attained for SNRs.

3.1. Synchrotron radio

Synchrotron radiation at the frequency $\nu = 1$ GHz is mainly emitted by electrons with energies $\sim 2(\nu/1 \text{ GHz})^{1/2}(B/100 \mu\text{G})^{-1/2} \text{ GeV}$. According to Ginzburg & Syrovatskii (1965), a flux $F_{\text{syn}}(\nu)$ of synchrotron radiation emitted from electrons with the broken power-law spectrum is

$$F_{\text{syn}}(\nu) = \frac{1}{4\pi d^2} \int \frac{\sqrt{3}e^3 B^{(\mu+1)/2} K_e}{2m_e c^2} \left(\frac{16m_e^3 c^5 \nu}{3e} \right)^{-(\mu-1)/2} \times \left[\int_{x_b}^{x_{\text{inj}}} F(x) x^{(\mu-3)/2} dx + E_b^{-\mu+\mu_2} \left(\frac{16m_e^3 c^5 \nu}{3eB} \right)^{(\mu-\mu_2)/2} \times \int_{x_{\text{max}}}^{x_b} F(x) x^{(\mu_2-3)/2} dx \right] 4\pi r^2 dr, \quad (10)$$

where

$$x = \frac{16m_e^3 c^5 \nu}{3eBE^2},$$

K_e is K of electrons (see Eq. (3)), d is the distance to the SNR, r is the radius from the center of the SNR, and $F(x)$ is the synchrotron function. The characters “inj”, “b”, and “max” are correspond to the injection, break, and maximum energy, respectively. Integration interval of r is given by the shocked ISM shell defined in the beginning of Section 3. Figure 4 shows the time evolution of the 1 GHz flux for the magnetic field in Figure 3. Since the blast wave is little decelerated, the radio flux continues to increase through ~ 10000 yr (see Section 4).

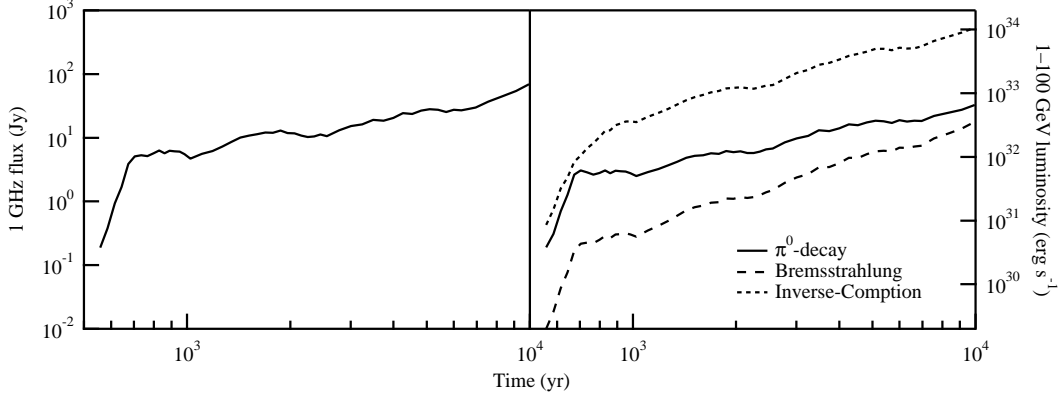


Fig. 4. *Left:* Radio flux at 1 GHz of synchrotron radiation from the blast-shocked ISM shell as functions of the elapsed time after explosion, calculated for $\xi_e = 10\xi_p$ and $d = 8$ kpc. *Right:* Luminosities of bremsstrahlung (broken), inverse-Compton scattering (dotted) and π^0 -decay (solid) γ -rays from the blast-shocked ISM shell in the 1–100 GeV band, as functions of the elapsed time after the explosion, calculated for $\xi_e = 10\xi_p$.

3.2. Bremsstrahlung γ -ray

Relativistic electrons emit bremsstrahlung γ -rays by interacting with target protons. Number of the bremsstrahlung photons emitted from electrons with the broken power-law spectrum per unit time per unit energy per unit volume is (Blumenthal & Gould 1970)

$$\begin{aligned} & \frac{dN_\gamma}{dtdh\nu dV} \\ &= \frac{4\alpha r_0^2 c n_T}{h\nu} \left[\ln \left(\frac{4h\nu}{m_e c^2} \right) - \frac{1}{2} \right] \\ & \times \int_{h\nu}^{E_{\max}} dE N_e E^{-2} \left[\frac{4}{3} E^2 - \frac{4}{3} E h\nu + (h\nu)^2 \right] \\ & \simeq 4\alpha r_0^2 c K_e n_T \left[\ln \left(\frac{4h\nu}{m_e c^2} \right) - \frac{1}{2} \right] \\ & \times \begin{cases} \frac{(3\mu^2 + \mu + 4)(h\nu)^{-\mu}}{3\mu(\mu-1)(\mu+1)} - \frac{4(\mu_2 - \mu)E_b^{-\mu+1}(h\nu)^{-1}}{3(\mu-1)(\mu_2-1)} \\ + \frac{4(\mu_2 - \mu)E_b^{-\mu}}{\mu\mu_2} - \frac{(\mu_2 - \mu)E_b^{-\mu-1}h\nu}{(\mu+1)(\mu_2+1)}, & h\nu \leq \frac{1}{2}E_b, \\ \frac{(3\mu_2^2 + \mu_2 + 4)(h\nu)^{-\mu_2}}{3\mu_2(\mu_2-1)(\mu_2+1)}, & h\nu > \frac{1}{2}E_b, \end{cases} \quad (11) \end{aligned}$$

where α is the fine structure constant, r_0 is the classical electron radius, h is the Planck constant, and n_T is the number density of target protons. The target protons are assumed to be thermal protons in the shocked ISM shell. We consider $E_{\max} \gg h\nu$ in the last expression in equation (11). Using equation (11), we get a bremsstrahlung γ -ray luminosity by

$$L_{\text{brems}} = \int \int h\nu \frac{dN_\gamma}{dtdh\nu dV} 4\pi r^2 dr d\nu. \quad (12)$$

Integration interval of r is given by the shocked ISM shell defined in the beginning of Section 3. We calculate the luminosity using $\langle n^2 \rangle$ obtained from hydrodynamical calculation of Paper I. Figure 4 shows the time evolution of γ -ray luminosity due to bremsstrahlung in the 1–100 GeV band.

3.3. Inverse-Compton γ -ray

When a photon of energy ϵ_0 is scattered by a relativistic electron of Lorentz factor γ , scattered photon has energy of $\sim \gamma^2 \epsilon_0$. Because the maximum energy of accelerated electrons is ~ 10 TeV, the electrons can emit photons of energies up to ~ 100 GeV by scattering cosmic microwave background (CMB) photons. Number of photons emitted from electrons with the broken power-law spectrum by scattering CMB photons of the temperature T_{CMB} per unit time per unit energy per unit volume is (Blumenthal & Gould 1970)

$$\begin{aligned} & \frac{dN_\gamma}{dtdh\nu dV} \\ &= \frac{8\pi^2 r_0^2 K_e E_b^{-\mu+\mu_2}}{h^3 c^2 (m_e c^2)^{\mu_2-1}} (kT_{\text{CMB}})^{(\mu_2+5)/2} \left[(h\nu)^{-(\mu_2+1)/2} \times \right. \\ & \frac{2^{\mu_2+3}(\mu_2^2 + 4\mu_2 + 11)}{(\mu_2 + 3)^2(\mu_2 + 5)(\mu_2 + 1)} \Gamma \left(\frac{\mu_2 + 5}{2} \right) \zeta \left(\frac{\mu_2 + 5}{2} \right) \\ & \left. - h\nu \frac{2^{\mu_2+2}\pi^2}{3(\mu_2 + 1)} \left(\frac{m_e^2 c^4}{4E_{\max,e}^2 kT_{\text{CMB}}} \right)^{(\mu_2+1)/2} \right], \quad (13) \end{aligned}$$

where ζ is the zeta function and $E_{\max,e}$ is the maximum energy of accelerated electrons. Using equation (13), we get an inverse-Compton γ -ray luminosity by

$$L_{\text{IC}} = \int \int h\nu \frac{dN_\gamma}{dtdh\nu dV} 4\pi r^2 dr d\nu. \quad (14)$$

Integration interval of r is given by the shocked ISM shell defined in the beginning of Section 3. Figure 4 shows the time evolution of the γ -ray luminosity due to inverse-Compton scattering in the 1–100 GeV band.

3.4. π^0 -decay γ -ray

Relativistic protons emit neutral π^0 s through inelastic collisions with protons, and then the π^0 s decays into two γ -ray photons. We calculate the π^0 -decay γ -ray luminosity, using the parameterized cross section of inelastic proton-proton collision

$$\sigma_{\text{inel}}(\tilde{E}_p) \simeq 3 \left[0.95 + 0.06 \ln \left(\frac{E_p}{1 \text{ GeV}} \right) \right] \times 10^{-26} \text{ cm}^2, \quad (15)$$

and δ -function approximation of number of π^0 s emitted per unit time per unit energy per unit volume

$$\begin{aligned} & \frac{dN_\pi}{dtd\tilde{E}_\pi dV} \\ &= \frac{cn_T}{f_\pi} \sigma_{\text{inel}} \left(m_p c^2 + \frac{\tilde{E}_\pi}{f_\pi} \right) N_p \left(m_p c^2 + \frac{\tilde{E}_\pi}{f_\pi} \right), \quad (16) \end{aligned}$$

which are used in Aharonian & Atoyan (2000). Here $f_\pi \simeq 0.17$ is mean fraction of the kinetic energy of proton transferred to π^0 per collision, $\tilde{E}_p = \gamma m_p c^2$ is total energy of proton and $\tilde{E}_\pi = \gamma m_\pi c^2$ is total energy of π^0 . Number of π^0 -decay photons emitted from protons with the broken power-law spectrum per unit time per unit energy per unit volume is

$$\begin{aligned} & \frac{dN_\gamma}{dtdh\nu dV} \\ &= 2 \int_{E_{\text{min}}}^{\infty} \frac{1}{(\tilde{E}_\pi^2 - m_\pi^2 c^4)^{1/2}} \frac{dN_\pi}{dtd\tilde{E}_\pi dV} d\tilde{E}_\pi \\ &\simeq 2 \int_{h\nu}^{\infty} \frac{1}{\tilde{E}_\pi} \frac{dN_\pi}{dtd\tilde{E}_\pi dV} d\tilde{E}_\pi \\ &\simeq 3 \times 10^{-26} \frac{2cn_T K_p}{f_\pi} \times \\ &\begin{cases} \frac{1}{\mu} \left(\frac{h\nu}{f_\pi} \right)^{-\mu} \left[0.95 + 0.06 \left(\ln \left(\frac{h\nu/f_\pi}{1 \text{ GeV}} \right) + \frac{1}{\mu} \right) \right] \\ + E_b^{-\mu} \left[0.95 \left(\frac{1}{\mu_2} - \frac{1}{\mu} \right) + 0.06 \left(\frac{1}{\mu_2^2} - \frac{1}{\mu^2} \right) \right. \\ \left. + 0.06 \left(\frac{1}{\mu_2} - \frac{1}{\mu} \right) \ln \left(\frac{E_b}{1 \text{ GeV}} \right) \right], \\ \text{for } h\nu \leq f_\pi E_b, \\ \frac{E_b^{-\mu+\mu_2}}{\mu_2} \left(\frac{h\nu}{f_\pi} \right)^{-\mu_2} \left[0.95 + 0.06 \left(\ln \left(\frac{h\nu/f_\pi}{1 \text{ GeV}} \right) + \frac{1}{\mu_2} \right) \right], \\ \text{for } h\nu > f_\pi E_b, \end{cases} \quad (17) \end{aligned}$$

where $E_{\text{min}} = h\nu + (m_\pi^2 c^4 / 4h\nu)$ is the minimum pion energy to produce photon of energy $h\nu$ and K_p is K of protons (see Eq. (3)). In the second expression in equation (17), $h\nu > m_\pi c^2$ and $\tilde{E}_\pi > m_\pi c^2$ are considered because we calculate photons above 1 GeV. In the last expression of equation (17), we approximate the proton energy spectrum as the relativistic form and the variable of the spectrum as $(m_p c^2 + \tilde{E}_\pi / f_\pi) \sim \tilde{E}_\pi / f_\pi$, because $\tilde{E}_\pi / f_\pi \gtrsim (1 \text{ GeV} / 0.17) \sim 6 \text{ GeV} > m_p c^2$. Using equation (17), we get a π^0 -decay γ -ray luminosity by

$$L_\pi = \int \int h\nu \frac{dN_\gamma}{dtdh\nu dV} 4\pi r^2 dr d\nu. \quad (18)$$

Integration interval of r is given by the shocked ISM shell defined in the beginning of Section 3. As in the calculation of the bremsstrahlung luminosity, we use $\langle n^2 \rangle$ instead of $\langle n \rangle^2$. Figure 4 shows the time evolution of γ -ray luminosity due to π^0 -decay in the 1–100 GeV band.

4. Discussion

For the low density ISM of density 0.016 cm^{-3} in the present model, supposed for an HII region (e.g., formed

by the progenitor and extended to a few tens pc), the blast wave is little decelerated through $\sim 10000 \text{ yr}$. As a result, in the context of diffusive shock acceleration described in Section 2, the radio flux continues to increase, because the increase of the emission measure overcomes the decrease of the magnetic field strength. Consequently, for about ten thousand years, recombination-radiation X-rays are observed from the irregular-shape inner part of SNR (see Figure 1 and Paper I), while the radio emission of tens Jy is observed from the blast-shocked ISM shell.

In the beginning of the Sedov/Taylor phase where the blast wave is being decelerated significantly as $V_s \propto t^{-3/5}$, the radio flux turns to decrease slowly as $t^{-3/10}$, and then approaches nearly constant as the magnetic field approaches its interstellar value ($\sim 3 \mu\text{G}$) and T_e approaches T_p . Also the inverse-Compton γ -rays turns to decrease as $\propto t^{-1/5}$ in the Sedov/Taylor phase, while π^0 -decay γ -rays are nearly constant. This sort of analysis is done also for the phase $\lesssim 10000 \text{ yr}$ with the relation $V_s \propto t^{-s}$ where s is given by the hydrodynamical calculation, and gives a good agreement with the computed time evolution of the radio and γ -ray emission in Figure 4. It should be noted that $s \sim 0.4$ at 10000 yr, yet smaller than the Sedov value $s = 3/5$, and the SNR is in the transient phase to the Sedov/Taylor regime.

Again because of low density, the γ -ray luminosity of the shocked ISM shell is dominated by inverse-Compton scattering through the SNR evolution concerned. However, π^0 -decay γ -rays could be enhanced by interactions with dense external matter, e.g., dense HI gas, molecular clouds or a cavity wall formed by the stellar wind of the progenitor. If 10% of accelerated protons interact with such matter of density $n \sim 100 \text{ cm}^{-3}$, the luminosity L_π would exceed $10^{35} \text{ erg s}^{-1}$ at a few thousands year, comparable to the typical γ -ray luminosity of MM SNRs. The interactions with molecular clouds are suggested in many MM SNRs by OH maser and/or near-infrared observations. The interaction with HI gas is suggested in RX J1713.7-3946 by observations (Fukui et al. 2012), and may be expected also in MM SNRs.

Interaction with some dense external matter may be realized on the γ -ray to radio flux ratio. We show the ratio of 1–100 GeV to 1 GHz flux in Figure 5. One can see that the ratio is systematically high for MM SNRs compared to shell-like SNRs except for RX J1713.7-3946 and Vela Jr. For RX J1713.7-3946 interaction with molecular clouds (e.g., Dame et al. 2001) and/or HI gas (Fukui et al. 2012) is suggested by observations. As for Vela Jr., an X-ray source CXOU J085201.4-461753, possible neutron star, is located near the center of the SNR (Pavlov et al. 2001). That might be related to the hard radio spectrum and high γ -ray/radio ratio, though the pulsar activity is not observed. The low ratio of Cas A is due likely to a strong field $\sim 1 \text{ mG}$ (e.g., Arbutina et al. 2012).

When electrons responsible for radio and electrons/protons for γ -rays are produced in the same volume, the γ -ray/radio ratio is reduced to $n_T / B^{3/2}$. Therefore, if the particle spectrum and B do not vary so much from SNR to SNR, the ratio can be a measure of the density

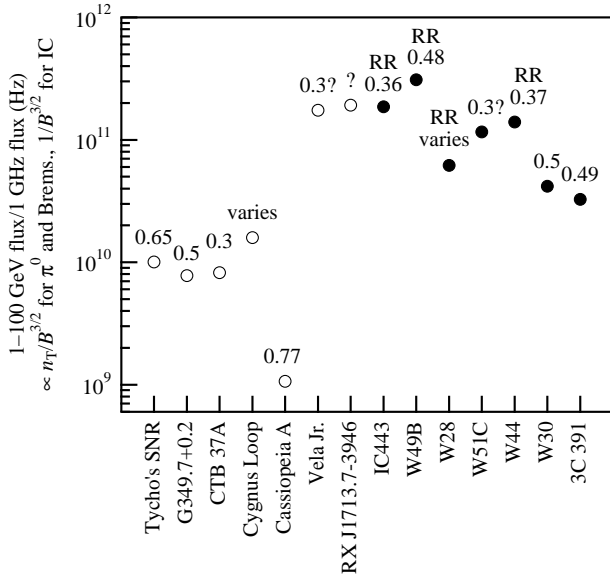


Fig. 5. Flux ratio of 1–100 GeV to 1 GHz of shell-like (open circles) and MM (filled circles) SNRs observed so far by *Fermi*. Attached numbers indicate the power indexes of the radio spectra (Green 2009) and “RR” means that recombination-radiation X-rays are observed.

References.—Radio flux of SNRs, except for RX J1713.7-3946 (Acero et al. 2009); Green 2009, γ -rays and distance: Tycho’s SNR; Hayato et al. 2010, Giordano et al. 2011, G349.7+0.2; Frail et al. 1996, Castro & Slane 2010, CTB 37A; Reynoso & Mangum 2000, Castro & Slane 2010, Cygnus Loop; Blair et al. 2005, Katagiri et al. 2011, Cassiopeia A; Reed et al. 1995, Abdo et al. 2010b, Vela Jr.; Katsuda et al. 2008, Tanaka et al. 2011, RX J1713.7-3946; Fukui et al. 2003, Abdo et al. 2011, IC443; Welsh & Sallmen 2003, Abdo et al. 2010c, W49B; Moffett & Reynolds 1994, Abdo et al. 2010e, W28; Velázquez et al. 2002, Abdo et al. 2010d, W51C; Koo et al. 1995, Abdo et al. 2009, W44; Wolszczan et al. 1991, Abdo et al. 2010a, W30; Fich et al. 1989, Castro & Slane 2010, 3C 391; Frail et al. 1996, Castro & Slane 2010

n_T of the matter with which the particles interact. For $B \sim 100 \mu\text{G}$ the high ratios observed from MM SNRs may be explained by π^0 -decay if the density of the target matter $n_T > 10 \text{ cm}^{-3}$, higher than the typical ISM density ($\lesssim 1 \text{ cm}^{-3}$). The high ratios could be explained also by inverse-Compton if $B \lesssim 10 \mu\text{G}$. Such a field may be possible for shell-like SNRs, but unlikely for MM SNRs which exhibit rather high radio flux.

Finally, we mention the effect of the CSM, stellar wind matter here. An important effect of the CSM is that the shock break-out raises the maximum energy E_{max} to $\sim 1300 \text{ TeV}$ for protons (see Figure 3). Since $E_{\text{max}} \propto BV_s^2 t \propto V_s^3 \propto (E_{\text{ej}}/M_{\text{ej}})^{3/2}$, where E_{ej} and M_{ej} are the initial kinetic energy of ejecta and the ejecta mass, respectively, E_{max} would reach $\sim 3000 \text{ TeV}$, the cosmic-ray knee energy, for 2 times larger value of $E_{\text{ej}}/M_{\text{ej}}$ than that in the present model.

We are grateful to Yutaka Ohira, Inoue Tsuyoshi and Ryo Yamazaki for meaningful discussion about particle acceleration. Also to the anonymous referee for his/her

careful reading the manuscript. KM and KK are respectively supported by the Grant-in-Aid for Scientific Research 22540253 and 24540229, from Japan Society for the Promotion of Science (JSPS).

References

- Abdo, A. A. et al. 2009, *ApJ*, 706, L1
 Abdo, A. A. et al. 2010a, *Science*, 327, 1103
 Abdo, A. A. et al. 2010b, *ApJ*, 710, L92
 Abdo, A. A. et al. 2010c, *ApJ*, 712, 459
 Abdo, A. A. et al. 2010d, *ApJ*, 718, 348
 Abdo, A. A. et al. 2010e, *ApJ*, 722, 1303
 Abdo, A. A. et al. 2011, *ApJ*, 734, 28
 Acero, F., Ballet, J., Decourchelle, A., Lemoine-Goumard, M., Ortega, M., Giacani, E., Dubner, G., & Cassam-Chenai, G. 2009, *A&A*, 505, 157
 Aharonian, F. A., & Atoyan, A. M. 2000, *A&A*, 362, 937
 Arbutina, B., Urošević, D., Andjelić, M. M., Pavlović, M. Z., & Vukotić, B. 2012, *ApJ*, 746, 79
 Bell, A. R. 1978, *MNRAS*, 182, 443
 Bell, A. R., & Lucek, S. G. 2001, *MNRAS*, 321, 433
 Berezhinskii, V. S., Bulanov, S. V., Dogiel, V. A., & Ptuskin, V. S. 1990, in *Astrophysics of Cosmic Rays*, ed. V. L. Ginzburg (Amsterdam: North-Holland), 62
 Blair, W. P., Sankrit, R., & Raymond, J. C. 2005, *AJ*, 129, 2268
 Blumenthal, G. R., & Gould, R. J. 1970, *Rev. Mod. Phys.*, 42, 237
 Castro, D., & Slane, P. 2010, *ApJ*, 717, 372
 Claussen, M. J., Frail, D. A., Goss, W. M., & Gaume, R. A. 1997, *ApJ*, 489, 143
 Dame, T. M., Hartmann, D., & Thaddeus, P. 2001, *ApJ*, 547, 792
 Dougherty, S. M., Clark, J. S., Negueruela, I., Johnson, T., & Chapman, J. M. 2010, *A&A*, 511, 58
 Ferrand, G., Decourchelle, A., Ballet, J., Teyssier, R., & Fraschetti, F. 2010, *A&A*, 509, L10
 Fich, M., Blitz, L., & Stark, A. A. 1989, *ApJ*, 342, 272
 Frail, D. A., Goss, W. M., & Slysh, V. I. 1994, *ApJ*, 424, L111
 Frail, D. A., Goss, W. M., Reynoso, E. M., Giacani, E. B., Green, A. J., & Otrupcek, R. 1996, *AJ*, 111, 1651
 Fukui, Y., et al. 2003, *PASJ*, 55, L61
 Fukui, Y., et al. 2012, *ApJ*, 746, 82
 Gal-Yam, A., et al. 2007, *ApJ*, 656, 372
 Ginzburg, V. L., & Syrovatskii, S. I. 1965, *ARA&A*, 3, 297
 Giordano, F. et al. 2012, *ApJ*, 744, L2
 Green, A. J., Frail, D. A., Goss, W. M., & Otrupcek, R. 1997, *AJ*, 114, 2058
 Green, D. A. 2009, *Bulletin of the Astronomical Society of India*, 37, 45
 Hayato, A., et al. 2010, *ApJ*, 725, 894
 Hewitt, J. W., & Yusef-Zadeh, F. 2009, *ApJ*, 694, L16
 Humphreys, R. M., & Davidson, K. 1994, *PASP*, 106, 1025
 Itoh, H., & Masai, K. 1989, *MNRAS*, 236, 885
 Katagiri, H. et al. 2011, *ApJ*, 741, 44
 Katsuda, S., Tsunemi, H., & Mori, K. 2008, *ApJ*, 678, L35
 Keohane, J. W., Reach, W. T., Rho, J., & Jarrett, T. H. 2007, *ApJ*, 654, 938
 Kiewe, M. et al. 2012, *ApJ*, 744, 10
 Koo, B.-C., Kim, K.-T., & Seward, F. D. 1995, *ApJ*, 447, 211
 Li, H., & Chen, Y. 2012, *MNRAS*, 421, 935
 Masai, K. 1994, *ApJ*, 437, 770
 Moffett, D. A., & Reynolds, S. P. 1994, *ApJ*, 437, 705

- Moriya, T. J. 2012, ApJ, 750, L13
- Ohnishi, T., Koyama, K., Tsuru, T. G., Masai, K., Yamaguchi, H., & Ozawa, M. 2011, PASJ, 63, 527
- Ozawa, M., Koyama, K., Yamaguchi, H., Masai, K., & Tamagawa, T. 2009, ApJ, 706, L71
- Pavlov, G. G., Sanwal, D., Kızıltan, B., & Garmire, G. P. 2001, ApJ, 559, L131
- Putze, A., Maurin, D., & Donato, F. 2011, A&A, 526, 101
- Reed, J. E., Hester, J. J., Fabian, A. C., & Winkler, P. F. 1995, ApJ, 440, 706
- Rho, J., & Petre, R. 1998, ApJ, 503, L167
- Reynoso, E. M., & Mangum, J. G. 2000, ApJ, 545, 874
- Sawada, M., & Koyama, K. 2012, PASJ, 64, 81
- Shimizu, T., Masai, K., & Koyama, K. 2012, PASJ, 64, 24
- Tanaka, T. et al. 2011, ApJ, 740, L51
- Uchida, H., et al. 2012, PASJ, 64, 141
- Uchiyama, Y., Aharonian, F. A., Tanaka, T., Takahashi, T., & Maeda, Y. 2007, Nature, 449, 576
- Velázquez, P. F., Dubner, G. M., Goss, W. M., & Green, A. J. 2002, AJ, 124, 2145
- Welsh, B. Y., & Sallmen, S. 2003, A&A, 408, 545
- Wolszczan, A., Cordes, J. M., & Dewey, R. J. 1991, ApJ, 372, L99
- Yamaguchi, H., Ozawa, M., Koyama, K., Masai, K., Hiraga, J. S., Ozaki, M., & Yonetoku, D. 2009, ApJ, 705, L6
- Yamauchi, S., Nobukawa, M., Koyama, K., & Yonemori, M. 2012, PASJ, 65, 6
- Yusef-Zadeh, F., Uchida, K. I., & Roberts, D. 1995, Science, 270, 1801